Surface Science 618 (2013) 20–26

Contents lists available at ScienceDirect

Surface Science

journal homepage: www.elsevier.com/locate/susc

Growth of ultrathin amorphous alumina films during the oxidation of NiAl(100)

Na Cai [a], Hailang Qin [a], Xiao Tong [b], Guangwen Zhou [a,*]

[a] Department of Mechanical Engineering & Multidisciplinary Program in Materials Science and Engineering, State University of New York, Binghamton, NY 13902, United States
[b] Center for Functional Nanomaterials, Brookhaven National Laboratory, Upton, NY 11973, United States

ARTICLE INFO

Article history:
Received 5 May 2013
Accepted 3 September 2013
Available online 16 September 2013

Keywords:
Ultrathin oxide film
NiAl
Alumina
Oxidation

ABSTRACT

The effect of temperature on the oxidation of NiAl(100) is comparatively studied at 25 °C and 300 °C using X-ray Photoelectron Spectroscopy to elucidate the effect of oxide–alloy interfacial reaction on the growth of ultrathin alumina thin films. The oxidation at 25 °C results in self-limiting aluminum oxide film growth to a less extent of the limiting thickness regimes with non-stoichiometric oxide films exhibiting a deficiency of Al cations, whereas for the oxidation at 300 °C the oxide films grow to a larger limiting thickness with relatively enriched with Al at the limiting thickness. The temperature dependent limiting thickness and composition of the oxide films are ascribed to the transport velocity of Al from deeper layers to the oxide/alloy interface during the oxide growth. For the oxidation at 25 °C the oxide film growth depletes Al and forms an underlying Ni-rich interfacial layer that blocks the supply of Al atoms to the oxide/substrate interface, whereas for the oxidation at 300 °C the enhanced diffusion rate maintains adequate supply of Al atoms to the oxide/alloy interface to sustain the oxide film growth to the full extent of the limiting thickness.

1. Introduction

Ultrathin oxide films on metal supports represent a unique combination of material systems with unprecedented properties and potential applications ranging from heterogeneous catalysis to electronic devices [1–16]. The distinct properties of ultrathin oxide films rely critically on the thickness and structure of the oxide films as they are grown on the metal substrates. For such material systems, the role of the metallic substrate goes far beyond that of a simple passive support because of its active participation in the film formation process and in the film properties, as exemplified by the ultrathin oxide film formation via directly oxidizing a metallic substrate. Exposure of a clean metallic surface (e.g. Al, Ta, Cr) to oxygen at relatively low temperatures (say <300 °C) often results in a self-limiting thin amorphous oxide, whereas at higher temperatures, thicker oxide films develop and the resulting structure of the corresponding oxide films is in most cases crystalline [17–20]. Thus, oxidation at relatively low temperatures is often employed to grow ultrathin oxide films with subsequent high-temperature vacuum annealing of the amorphous oxide films for improved structural ordering. Usually, the temperature required to order the oxide film is much higher than the melting temperature of the elemental metal. An advantage of using intermetallic alloys for thin oxide film formation is that higher annealing temperatures can be used to order the film without melting the substrate.

In this context, oxidation of NiAl alloys has received extensive interest for its ability to form well-ordered Al_2O_3 film by selective oxidation of Al [21–31]. Controlled growth of Al_2O_3 films has great importance. For instance, the use of Al_2O_3 thin films grown on conducting substrates can avoid charging problems and greatly facilitates the study of heterogeneous catalysis with electron spectroscopic techniques. In addition, Al_2O_3 is a wide gap insulating material and holds great potential as an insulating layer for nano-electronics. Developing experimental control with respect to thickness, structure and stoichiometry of the oxide films would allow these structural properties to influence their functionalities [1]. Nearly all metals form a passivation film due to oxidation at ambient temperature. The classic theory of Cabrera and Mott describes why metals form such a self-limiting oxide film at low temperatures [32]. Since the growth of the oxide film at low temperatures (e.g. room temperature) is not thermally activated, Cabrera–Mott theory proposes that ionic diffusion through the oxide film is driven by a self-generated electric field across the oxide film resulting from electron tunneling between the Fermi level of the parent metal and acceptor levels of chemisorbed oxygen at the oxide surface. The self-generated electric field reduces the energy barrier for ion migration through the oxide film, leading to rapid initial oxidation rates at low temperature. Since the tunneling current decreases exponentially with increasing oxide film thickness, the oxidation essentially stops at a limiting thickness. Such an interplay between the electronic interaction and mass transfer thus provides unique opportunities to explore various combinations of a metal/oxide system to tune the oxide film growth. To achieve this goal, the processes that take place in the developing oxide film and at the oxide/substrate interface during the oxide film

* Corresponding author.
E-mail address: gzhou@binghamton.edu (G. Zhou).

0039-6028/$ – see front matter © 2013 Elsevier B.V. All rights reserved.
http://dx.doi.org/10.1016/j.susc.2013.09.011

growth have to be elucidated, and the fundamental knowledge of the relationship between the mechanism that governs the oxide-film growth and the resulting chemical composition, thickness, and morphology should be established.

Using X-ray Photoelectron Spectroscopy (XPS), we demonstrate in this work that the limiting thickness of a Al_2O_3 thin film during the oxidation of a NiAl(100) surface can be controlled by either oxygen pressure or oxidation temperature. We particularly focus on the relationships between the oxide-film growth kinetics and the evolution of the chemical composition and chemical state as a function of the oxidation temperature and oxygen pressure. Detailed analyses of the spectral features and binding energy reveal that the stoichiometry and limiting thickness of the oxide film bear a strong dependence on the growth conditions (i.e., oxidation temperature and oxygen pressure). These results suggest that the self-limiting growth of the oxide films depends on not only the establishment of the Mott potential across the oxide film resulting from the electron tunneling effect to control the atom transport in the oxide overlayer but also the transport velocity of atom by bulk diffusion in the alloy substrate. The study of gaining a control over the growth of an ultrathin oxide film such as the thickness and composition provides a baseline from which the range of temperature and pressure can be pursued to grow ultrathin Al_2O_3 thin film with tuned reactivity and functionality.

2. Experimental

The experiments were carried out in an ultrahigh vacuum (UHV) chamber equipped with an X-ray Photoelectron Spectroscopy (XPS) — SPECS Phiobos 100MCD analyzer, low energy electron diffraction (LEED), scanning tunneling microscopy (STM), and an Ar-gas ion sputtering gun. The chamber has a typical base pressure of 2×10^{-10} Torr. A non-monochromatized Al–Kα X-ray source ($h\nu = 1486.6$ eV) was used for the XPS studies. The NiAl(100) single crystal is a 'top-hat' disk (1 mm thick and 8 mm in diameter), purchased from Princeton scientific Corp., cut to within 0.1° to the (100) crystallographic orientation and polished to a mirror finish. The sample was heated via a ceramic button heater and its temperature monitored with a type-K thermocouple. The crystal was cleaned by cycles of Ar^+ sputtering at 25 °C (5×10^{-6} Torr of Ar^+, 1 μA cm^{-2}, 1.0 KeV) followed by annealing at 960 °C. Surface cleanliness was checked with XPS. Surface morphology and crystallinity of the oxidized NiAl(100) surface were examined by STM and LEED.

Oxygen gas (purity = 99.9999%) was introduced to the system through a variable pressure valve and the oxide layers were grown in the sample preparation chamber as a function of oxygen exposure time under controlled oxygen pressure (pO_2) at the two substrate temperatures T = 25 °C and 300 °C. All the oxidation experiments executed in this study were performed on the same NiAl(100) crystal. Before each oxidation experiment, the oxidized NiAl surface was fully cleaned and its crystallinity was restored by the treatment of sputtering and subsequent annealing, as confirmed by XPS and LEED. Spectra of the Al(2p), Ni(2p), Ni(3p), and O(1s) were recorded before and after oxidation. In order to compare the stoichiometry of the oxide films with that of bulk material, the composition of the oxide film, expressed as its Al/O atomic ratio, was determined from the total photoelectron intensity ratio of the oxidic Al(2p) peak and the O(1s) peak of XPS spectra obtained from the oxidized NiAl. An absolute stoichiometric composition for each film can be calculated by using a reference XPS spectrum. Here the experimental XPS spectra of a well-defined oxide thin film formed by oxidizing NiAl(110) (O:Al = 13:10) [21] from our system are used. The thickness of the developing oxide overlayer is estimated from the attenuation of the metallic Al(2p) XPS peak with films with the photoelectron attenuation length for Al_2O_3 ($\lambda = 16.7 \pm 0.6$ Å) [33,34] by using the formula $d = -\lambda \cos\theta \ln\left(\frac{A}{A_0}\right)$, where A is the area of Al metallic peak after oxygen exposure, A_0 is the area of the Al metallic peak before oxygen exposure, λ is the inelastic mean free path and θ is the angle between analyzer and the sample surface normal, 0° in our case.

3. Results

The freshly cleaned NiAl(100) is oxidized with water vapor at the pressures varying from 1×10^{-8} Torr to 10 Torr at two temperatures: 25 °C and 300 °C. For each oxygen pressure and temperature, a limiting oxide film thickness is reached after long time exposure. XPS measurements are performed with the NiAl(100) surface being exposed to different oxygen pressures for different time periods. The Al(2p), Ni(2p), Ni(3p) and O(1s) XPS spectra are monitored to investigate the changes in spectral features and binding energies due to the oxidation. Fig. 1 shows the representative XPS spectra of Ni 2p core level peaks obtained from a freshly cleaned NiAl(100) surface, the NiAl(100) surface oxidized to the limiting thickness of the oxide film at T = 25 °C in $pO_2 = 1 \times 10^{-5}$ Torr, and the NiAl(100) surface oxidized to the limiting thickness of the oxide film at 300 °C in $pO_2 = 1 \times 10^{-5}$ Torr, respectively. The shape and position of the Ni 2p core level peak remains all the same for the different oxidation conditions. In addition, no oxidic Ni 2p peaks are observed at higher binding energies, indicating that Ni is not oxidized and remains in its metallic state under the oxidation conditions examined. However, the intensity of the Ni 2p peak decreases due to the oxidation, suggesting that the NiAl surface develops an alumina overlayer and its thickness increases with increasing the oxidation temperature.

Fig. 2 illustrates the representative XPS spectra of the corresponding Al 2p and Ni 3p core level peaks obtained from the NiAl(100) surfaces that are oxidized to the limiting thickness for the different oxygen pressures. Fig. 2(a) shows the oxidation at 25 °C and Fig. 2(b) corresponds to the oxidation at 300 °C. The positions of the metallic Al 2p peak and Ni 3p peak are constant while their intensities decrease with increasing the oxygen pressure for both temperatures. On the other hand, an oxidic Al 2p peak at a higher binding energy becomes visible. For the oxidation at 25 °C, the Al 2p intensity remains almost unchanged for increasing the oxygen pressure from 1×10^{-8} Torr to 1×10^{-5} Torr, whereas it increases appreciably for the oxidation at 300 °C with increasing the oxygen pressure, suggesting the dependence of the limiting thickness of the oxide film on both the oxygen pressure and temperature (as shown later, for the oxidation at T = 25 °C, a significantly large oxygen pressure of 10 Torr is needed in order to reach the similar limiting thickness of the oxide film attained for the oxidation at 300 °C and 1×10^{-5} Torr). Combining the results of the XPS peak positions illustrated in Figs. 1 and 2, we can conclude that under the range of

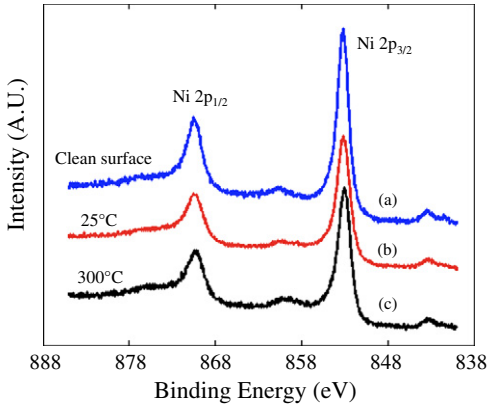

Fig. 1. Photoemission spectra of the Ni 2p core level region obtained for the pre-oxidized and oxidized NiAl(100) surfaces, (a) the freshly cleaned surface, (b) oxygen exposure at $pO_2 = 1 \times 10^{-5}$ Torr and T = 25 °C for 285 min, and (c) oxygen exposure at $pO_2 = 1 \times 10^{-5}$ Torr and T = 300 °C for 300 min.

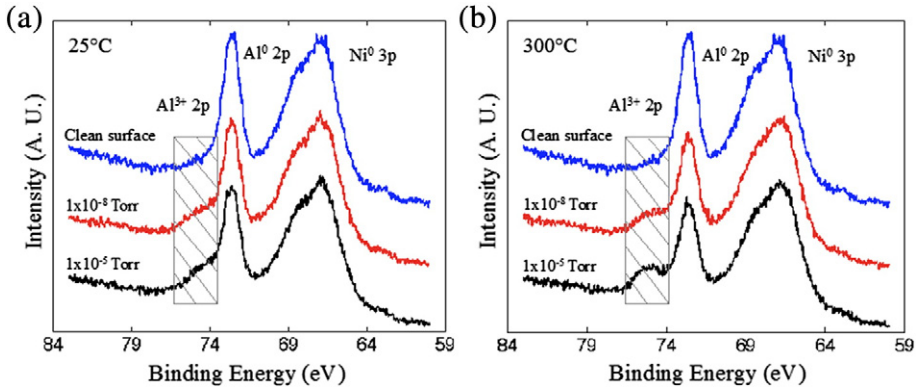

Fig. 2. Photoemission spectra of the Al 2p and Ni 3p core level regions for the freshly cleaned NiAl(100) surface and after extended exposures to oxygen gas at the indicated oxygen pressures and oxidation temperature (a) T = 25 °C and (b) T = 300 °C.

temperatures and oxygen pressures investigated the oxide film growth involves selective oxidation of Al in the NiAl alloy to form an alumina overlayer.

Fig. 3 shows the photoemission spectra of the Al 2p and Ni 3p core level peaks from the oxide films after attaining their limiting thickness. The positions of the metallic Al 2p peak remain almost constant for the temperatures of 25 °C and 300 °C. In contrast, the Ni 3p peak measured from the oxidation at 300 °C shifts to a lower binding energy (=66.38 eV) compared to that of 25 °C (=66.56 eV), which may suggest a change in the alloy composition. Bulk NiAl exhibits both ionic and covalent bonding due to a loss of electron density at the Al positions and gain at the Ni positions [35], which is expected from the different electronegativities of Ni (=1.9) and Al (=1.5). Compared to pure Ni, a smaller binding energy can be expected for Ni in NiAl because the increase in electron density at Ni sites increases the Coulomb repulsion with the cores and thus reduces the binding energy. From the energetic shift of the metallic Ni 3p peak, it can be thus inferred that a Ni-rich layer is developed at the oxide/substrate interface for the oxidation at 25 °C while a more stoichiometric NiAl is formed at the oxide/substrate interface for the oxidation at 300 °C.

Fig. 3 also shows the binding energy shift of the oxidic Al 2p peak for the different temperatures. Compared to the oxide film formed at 25 °C, the oxidic Al 2p peak measured from the oxidation at 300 °C shifts to a higher binding energy, i.e., the oxidic Al 2p peak appears at 74.35 eV for the oxide film formed at 25 °C while at 75.79 eV for the oxide thin film formed at 300 °C. This trend of the oxidic Al 2p peak shift toward a higher binding energy with increasing the oxidation temperature is also observed in the O 1s peak position. Fig. 4 illustrates the representative photoemission spectra of the O 1s core level region from the oxide films attaining the limiting thickness during oxidation at 25 °C and 300 °C, respectively. The O 1s peak maximum for the oxide film formed from the oxidation at 25 °C is located at 531.23 eV, whereas for the oxidation at 300 °C it has the O 1s peak maximum at the binding energy of 531.79 eV. This observed energetic shift is in agreement with temperature-dependent oxidation experiments performed on Al, where a difference in binding energy of up to 0.56 eV for both the oxidic Al 2p and O 1s lines was reported for alumina films formed at room temperature compared to those at 600 °C [36,37].

Fig. 5 shows the kinetic growth curves of the oxide film during the oxidation at 25 °C measured with XPS over a time period extending to approximately 4 h for each oxygen pressure. The oxygen gas exposure was interrupted for the XPS measurements. The oxidation starts with a clean NiAl(100) surface which is oxidized first at $pO_2 = 1 \times 10^{-8}$ Torr. The oxide film shows an initial fast growth stage, followed by a drastic reduction of the oxide film growth at longer times to the limited growth regime. Once no further changes in the oxide thickness were detected, stepwise increase in oxygen pressure was applied, resulting in no further oxide growth, irrespective of the prolonged oxygen exposure at these pressures, as shown in Fig. 5. Until the oxygen pressure was raised to 10 Torr, the oxide film growth was observed to take place again and reach a new limiting thickness.

Fig. 6 shows the kinetic growth curves of the oxide film as a function of time and oxygen pressure for the oxidation at 300 °C. The oxidation starts with a clean NiAl(100) surface at the oxygen pressure $pO_2 = 1 \times 10^{-8}$ Torr. Similarly, an initial fast growth stage occurs, followed by a reduction in growth rate to a limiting thickness of ~4.5 Å, which is thicker than the limiting thickness (~3.8 Å) of the oxide film for the

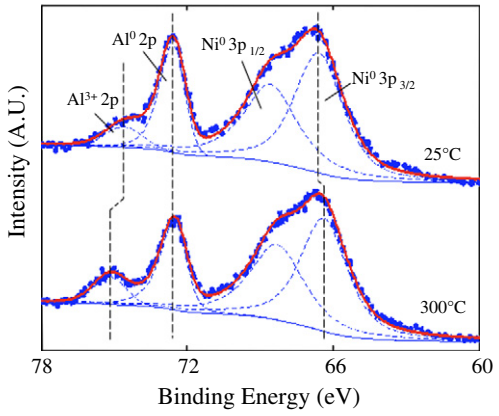

Fig. 3. Photoemission spectra of the Al 2p and Ni 3p regions for extended oxygen exposure at 25 °C and 300 °C. The Al^{3+} 2p peak shifts to a higher binding energy and Ni^0 $3p_{3/2}$ peak shifts to a lower binding energy as revealed by the deconvoluted peaks for the oxide films.

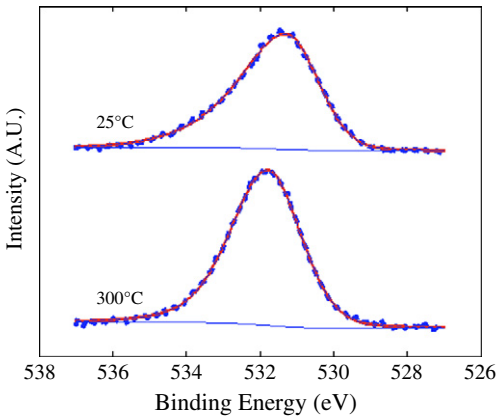

Fig. 4. Photoemission spectra of the O 1s region for extended oxygen exposure at 25 °C and 300 °C.

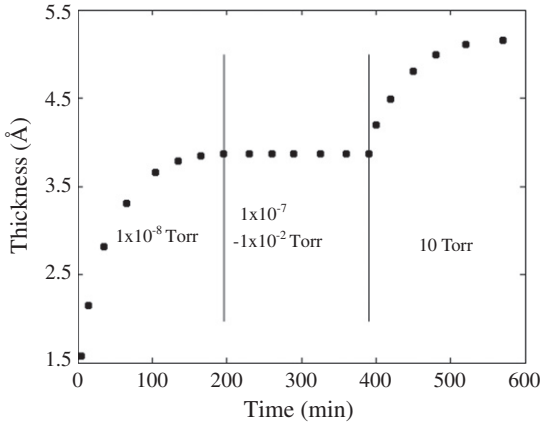

Fig. 5. Oxide film thickness as a function of oxidation time and oxygen gas pressure during the oxidation of NiAl(100) at T = 25 °C. The oxidation starts with a freshly cleaned NiAl(100) surface which is oxidized first at $pO_2 = 1 \times 10^{-8}$ Torr. Stepwise increase in oxygen pressure results in no further oxide growth until the pressure of $pO_2 = 10$ Torr is reached that leads to the oxide film growth to a new limiting thickness.

oxidation at 25 °C under the same oxygen pressure. Further increase in the oxygen pressure to $pO_2 = 1 \times 10^{-7}$ Torr and then to $pO_2 = 1 \times 10^{-6}$ Torr results in no additional oxide growth despite the prolonged oxygen exposures at these pressures. Until the oxygen pressure is raised to $pO_2 = 1 \times 10^{-5}$ Torr, the oxide film growth takes place again and reaches a new limiting thickness of ~5.4 Å. Due to the limitation by the experimental apparatus, the oxidation at the oxygen pressure higher than 1×10^{-5} Torr was not examined at the elevated temperature. By comparing with the oxide-film growth curves shown in Figs. 5 and 6, it can be seen that the oxide film growth to the similar limiting thickness at 300 °C occurs at a much smaller oxygen pressure (i.e., 1×10^{-5} Torr) compared to the oxidation at 25 °C, suggesting that the oxide film growth is significantly enhanced at the elevated oxidation temperature. It is also noted that this limiting thickness (5.4 Å) of the oxide film formed at 300 °C is smaller than that on an Al substrate, which has the limiting thickness of ~7.5 Å under the similar oxidation condition [20]. This difference is presumably due to the less amount of Al atoms present on the NiAl surface compared to a pure Al substrate.

The growth morphology and crystallinity of the oxide films on the NiAl(100) surface are also examined by STM and LEED. Fig. 7 shows the typical topographical STM images obtained from a clean NiAl(100)

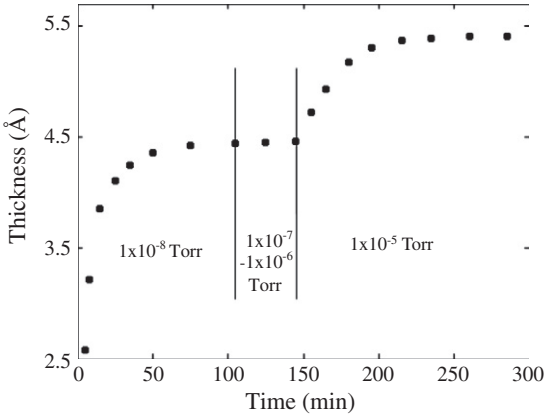

Fig. 6. Thickness evolution of the oxide film on NiAl(100) as a function of oxidation time and oxygen gas pressure at T = 300 °C. The oxidation starts with a clean NiAl(100) surface which is oxidized first at $pO_2 = 1 \times 10^{-8}$ Torr. A stepwise increase in oxygen pressure results in no further oxide growth until the pressure of $pO_2 = 1 \times 10^{-5}$ Torr is reached that leads to the oxide film growth to a new limiting thickness.

surface, the NiAl(100) surfaces oxidized at 25 °C, and the NiAl(100) surface oxidized at 300 °C, respectively. As seen in Fig. 7(a), the clean surface shows large flat terraces separated by a 3-Å atomic height step. This step height corresponds to the Al–Al separation in <001> direction (the lattice constant of NiAl = 2.89 Å). After the oxidation at 25 °C, the surface is flat and surface steps are still visible with the same step height of 3 Å. The morphology of the entire surface shows featureless amorphous material (Fig. 7(b)). The unchanged step height of 3 Å after the oxidation suggests the formation of a uniform amorphous layer over the entire surface across the upper and lower terraces. Fig. 7(c) shows a typical STM image obtained from the NiAl(100) oxidized at 300 °C. The surface morphology appears similar amorphous feature. The thickness of the oxide film formed at 300 °C is also uniform across the surface, as evidenced by the retained atomic height (3 Å) of the surface step after the oxidation. The corresponding LEED patterns obtained from these oxide films are diffuse or simply non-existent, further confirming that the oxide films formed at the two oxidation temperatures are amorphous in nature.

4. Discussion

The experimental results presented above reveal that the NiAl alloy exhibits selective oxidation, in which only Al participates in the formation of the oxide film. From a thermodynamic point of view the formation of an Al_2O_3 oxide layer is energetically strongly favored over the formation of a NiO overlayer because the heat of formation for Al_2O_3 (−1690.7 kJ/mol) is by a factor of seven larger than the corresponding value for NiO (−240.8 kJ/mol) [22,38]. Al_2O_3 formation on the NiAl surface results in free Ni atoms that can accumulate at the oxide/alloy interface or dissolve in the NiAl bulk through heating because the thermodynamically more stable phase in the NiAl system is the Ni-rich Ni_3Al. When the NiAl alloy is oxidized at the ambient temperature (i.e., 25 °C), all Al atoms available in the near-surface region will react with oxygen to form Al_2O_3. However, the Al bulk diffusion rate at this temperature is certainly too low to compensate the loss of Al at the surface instantaneously. Therefore, a Ni-enriched layer is developed at the oxide/substrate interface region. For oxidation at 300 °C, Ni dissolves into the bulk and Al segregation to the oxide/substrate interface. Thus, the room-temperature oxidation results in an Al-depleted region at the oxide/alloy interface, while the diffusion rate at the higher oxidation temperature is sufficient to maintain an equilibrium stoichiometry at the oxide/alloy interface. Fig. 8 shows schematically the temperature-dependent composition of the interface region, which corroborates well with the temperature-dependent binding energy of the metallic Ni 3p peak as shown in Fig. 3.

To confirm the speculated temperature-dependent interfacial composition described above, the development of two quantities, i.e., the intensity of the O 1s peak and the thickness of the oxide overlayer determined using the attenuation of the metallic Al 2p peak, is compared as a function of the oxide thickness. If the thickness of the oxide film is small compared to the photoelectron escape depth (this is indeed the case for our experiments, where the maximum film thickness is about 5.5 Å, which is much smaller than the attenuation length, $\lambda = 16.7 \pm 0.6$ Å, for electrons in Al_2O_3), the oxygen signal and the overlayer thickness should have a linear relation [33]. This holds for the oxidation at 300 °C, as shown in Fig. 9(a), where proper scaling of the integral intensity of the O1s peak makes it coincide closely to the thickness curves of the oxide film, which suggests Al segregation to the oxide/substrate interface to compensate the consumed Al atoms for the oxide formation.

However, such a coincidence does not happen for the oxidation at 25 °C. As seen in Fig. 9(b), the integral intensity of the O1s peak starts to deviate appreciably from the thickness curve of the oxide film at the oxide film thickness greater than ~2.75 Å. This suggests that the overlayer, which damps the XPS signal of the metallic Al 2p peak, cannot consist of pure oxide only. Thus, we conclude that the room-

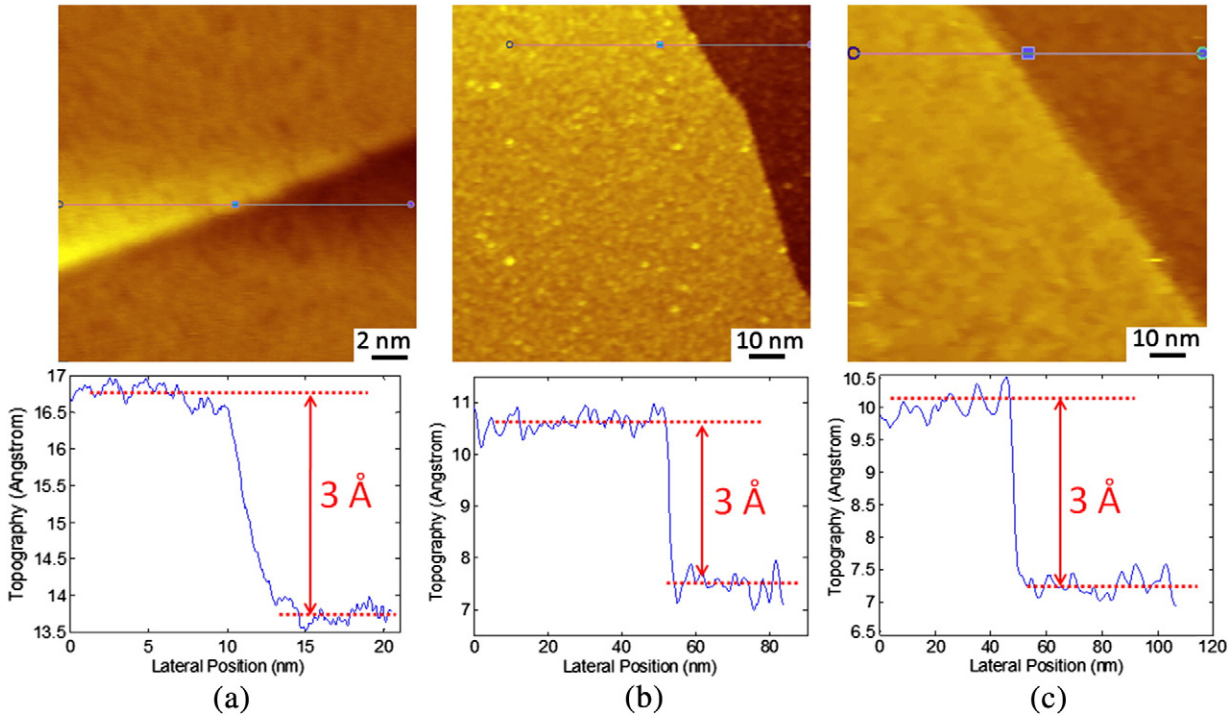

Fig. 7. Topographic STM images corresponding to: (a) the bare NiAl(100) surface, exhibiting terraces separated with a step height of 3 Å estimated by line profile (lower panel); (b) the surface oxidized at T = 25 °C and $pO_2 = 1 \times 10^{-8}$ Torr; and (c) the surface oxidized at T = 300 °C and $pO_2 = 1 \times 10^{-8}$ Torr.

temperature oxidation depletes the surface Al atoms, resulting in the formation of an interfacial Ni-rich layer that contributes to the damping of the XPS signal of the metallic Al. As a consequence, the true thickness of the oxide film for the oxidation at room temperature should be somewhat smaller than that determined by the attenuation formula due to the contribution from the Ni-rich region (their difference is about up to 8% as estimated using the linear dependence of the intensity of the O 1s peak on the oxide film thickness). Such a similar behavior of the temperature-dependent interfacial composition was observed from the XPS study of the oxidation of FeAl surfaces [33].

It should be noted that estimation of the thickness of the Ni-layer at the interface using the XPS data is quite challenging due to the uncertainty in quantifying the dampening of the metallic Al 2p peak by the Ni layer. The XPS Ni-spectra obtained from the oxidation at 25 °C and 300 °C are quite similar at the same film thickness, probably due to the much smaller thickness of the Ni layer (one or two top atom layers) compared to the sampling depth for XPS (several nm below the interface). Therefore, we used the O 1s and Al 2p peaks to infer the interfacial composition evolution, as described above. It would be beneficial if complementary in situ techniques capable of detecting the buried oxide/substrate interface region can be employed to determine the evolution of the interface composition and thickness under such dynamic oxidation conditions.

Table 1 summarizes the binding energies of the oxidic Al 2p and O 1s maxima (i.e., Figs. 3 and 4) and the Al/O atomic ratios obtained from the oxide films at their limiting thicknesses at 25 °C and 300 °C. The peak maxima shift to higher binding energies at the higher oxidation temperature. In general, the amount of a chemical shift is known to scale rather well with the number of heterogeneous chemical bonds, a larger chemical shift can be attributed to a larger coordination number (on average). For the oxidation at room temperatures, the amorphous aluminum oxide films can be described by a close packing of oxygen anions with the Al cations distributed over the octahedral and/or tetrahedral interstices and exhibit a deficiency of Al cations [18–20,36,39]. Indeed, the stoichiometry of the oxide films formed from the oxidation at 25 °C is approximately $Al_{(2-x)}O_3$ where x ~ 0.24, as determined from the XPS Al/O peak intensity ratio. For the oxidation at 300 °C the oxide films become relatively enriched with Al and have nearly stoichiometric alumina films at the limiting thickness, suggesting that the concentration of Al cations increases with increasing temperature. For both temperatures, the compositions are practically independent of the oxygen pressure. Thus, the chemical shift toward a higher binding energy would reflect

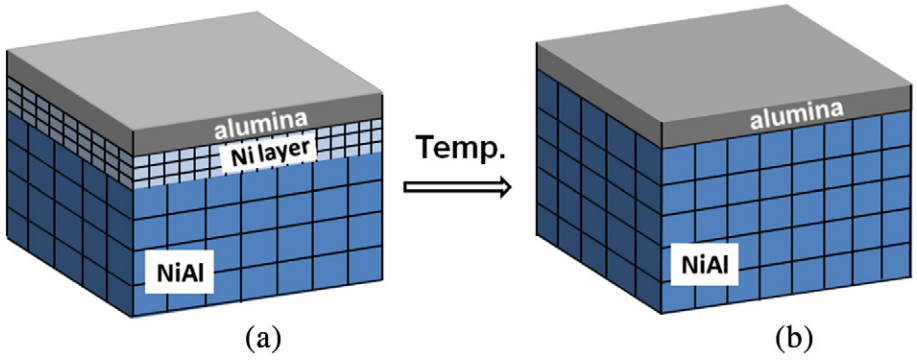

Fig. 8. Schematic illustration of the temperature-dependent composition at the oxide/alloy interface, (a) 25 °C and (b) 300 °C.

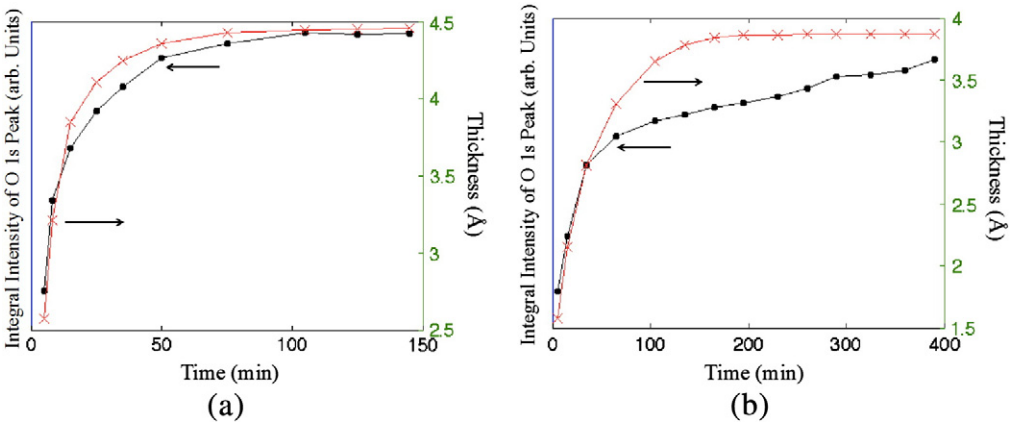

Fig. 9. Comparison of the integral intensity of the O 1s peak (left axis) with the overlayer thickness determined using the attenuation of the metallic Al 2p peak as a function of the oxidation time at (a) T = 300 °C and (b) T = 25 °C.

the development of a more compact alumina film with increased coordination numbers with increasing oxidation temperature.

The observed initially fast oxidation rate followed by a drastic reduction of the oxide film growth reaching a limiting oxide-film thickness at the two oxidation temperatures (Figs. 5 and 6) is typical for oxide-film growth under influence of the electric field setup by the negative oxygen ions chemisorbed onto the oxide surface due to electron tunneling through the oxide film (i.e., the Cabrera–Mott model of low temperature metal oxidation). The observed deficiency of Al cations at 25 °C and increase of Al cation concentration in the oxide film with increasing the oxidation temperature (i.e., 300 °C) suggests that the oxide film growth is governed by the electric-field controlled outward diffusion of Al cations through the developing oxide films. Indeed, the observed oxide-film growth kinetics are in line with previous studies on the kinetics of oxide-film growth on Al substrates, which showed that the oxidation at temperatures ≤300 °C exhibits self-limiting oxide film growth controlled by electric-field driven outward diffusion of Al cations through a close packing of oxygen anions in the amorphous oxide films [20].

For the self-limiting oxide film growth controlled by the electric-field driven diffusion, it was shown that the actual value of the Mott potential (and thus the strength of the self-generated electric field) is correlated with the oxygen anion coverage which can be well-described by a Langmuir isotherm dependence on the oxygen pressure and oxidation temperature [40–42]. For instance, under a constant oxygen pressure a higher oxidation temperature results in a thinner limiting thickness of the oxide film on Al(111) due to a reduction of the sticking coefficient of oxygen on the surface with increasing oxidation temperature [42]. This is in contrast with the observed behavior of the oxide film growth on the NiAl(100) surface shown here, for which the limiting thickness of the oxide films increases for the higher oxidation temperature. As noted from Figs. 5 and 6, an increase in oxygen pressure by six orders of magnitude (i.e., $pO_2 = 10$ Torr) is required for oxidation at 25 °C in order to reach the similar oxide-film limiting thickness attained by the oxidation at 300 °C and $pO_2 = 1 \times 10^{-5}$ Torr.

Such a temperature effect on the limiting thickness of the oxide films would be understood by considering the transport velocity of Al from deeper layers to the oxide/alloy interface during the oxide growth. As schematically shown in Fig. 8, the selective oxidation of Al results in an underlying Ni-enriched interfacial layer. This enrichment, in turn, requires the mass transport of material to and from the bulk, i.e., dissolution of Ni into the bulk and segregation of Al to the oxide/substrate interface, for continued oxide film growth. For the oxidation at room temperature, however, the topmost 1–2 Å of the alloy surfaces of Al is depleted, resulting in a Ni layer that blocks further supply of Al atoms to the oxide/substrate interface. Thus, despite of the larger oxygen sticking coefficient at the lower temperature that facilitates the development of a stronger Mott potential for field-driven diffusion in the oxide film, the oxide film grows to a less extent of the limiting thickness due to the depletion of Al at the oxide/alloy interface. For the oxidation at 300 °C, the diffusion of Al that has reacted to form oxide is adequately counterbalanced by Ni diffusion in the opposite direction toward the bulk, thereby sufficiently maintaining an equilibrium stoichiometry at the oxide/alloy interface. Thus, the oxide film is governed truly by the electric-field-controlled diffusion of Al through the oxide film due to the supply of sufficient Al atoms to the oxide/alloy interface to sustain the oxide film growth to the full extent of the limiting thickness that is commensurate with the Mott potential developed at the temperature and pressure.

Table 1
Binding energies of oxidic Al 2p, O 1s, and Al/O atomic ratio of the oxide films at their limiting thickness for the different temperatures investigated.

Temperature (°C)	25	300
Al (2p) (eV)	74.35	74.79
O(1s) (eV)	531.23	531.79
Al/O	0.0558	0.0650

5. Conclusions

We report a comparative study of the ultrathin amorphous alumina film growth during the oxidation of NiAl(100) at 25 °C and 300 °C. The oxide films formed from the oxidation at 25 °C exhibit Al deficiency while the oxide films from the oxidation at 300 °C become relatively enriched with Al with the nearly stoichiometric bulk alumina. Although oxide film growth kinetics for both the temperatures show a self-limiting growth behavior, the oxide films formed at the lower temperature grow to a less extent of the limiting thickness regimes due to depletion of Al atoms at the oxide/alloy interface, whereas the oxidation at the higher temperature results in the oxide film growth to the full extent of the limiting thickness for the enhanced diffusion rate of Al atoms in the NiAl alloy that is capable of supplying sufficient Al atoms from deeper layers to the oxide/alloy interface.

Acknowledgment

We acknowledge support from the National Science Foundation grant no. CBET-0932814. Research was carried out in part at the Center for Functional Nanomaterials, Brookhaven National Laboratory, which is supported by the U.S. Department of Energy, Office of Basic Energy Sciences, under contract no. DE-AC02-98CH10886.

References

[1] H.-J. Freund, Surf. Sci. 601 (2007) 1438.
[2] M. Bibes, J.E. Villegas, A. Barthelemy, Adv. Phys. 60 (2011) 5.
[3] L. Giordano, G. Pacchioni, Acc. Chem. Res. 44 (2011) 1244.
[4] S. Shaikhutdinov, H.-J. Freund, Annu. Rev. Phys. Chem. 63 (2012) 619.
[5] S. Altieri, L.H. Tieng, G.A. Sawatzky, Thin Solid Films 400 (2001) 9.
[6] M.S. Chen, D.W. Goodman, J. Phys. Condens. Matter 20 (264013) (2008)(11 pp.).
[7] Q. Fu, T. Wagner, Surf. Sci. Rep. 62 (2007) 431.
[8] H.-J. Freund, G. Pacchioni, Chem. Soc. Rev. 37 (2008) 2224.
[9] G.L. Haller, D.E. Resasco, Adv. Catal. 36 (1989) 173.
[10] O. Dulub, W. Hebenstreit, U. Diebold, Phys. Rev. Lett. 84 (2000) 3646.
[11] D.W. Goodman, Surf. Rev. Lett. 9 (1995) 109.
[12] H.-J. Freund, Surf. Sci. 500 (2002) 271.
[13] U. Diebold, Surf. Sci. Rep. 48 (2003) 53.
[14] W. Monch, Rep. Prog. Phys. 53 (1990) 221.
[15] D.W. Goodman, Catal. Lett. 99 (2005) 1.
[16] U. Diebold, J.M. Pan, T.E. Madey, Surf. Sci. 845 (1995) 331.
[17] F.P. Fehlner, Low-Temperature Oxidation, John Wiley & Sons, Inc., New York, 1986.
[18] L.P.H. Jeurgens, W.G. Sloof, F.D. Tichelaar, E.J. Mittemeijer, Phys. Rev. B 62 (2000) 4707.
[19] L.P.H. Jeurgens, W.G. Sloof, F.D. Tichelaar, E.J. Mittemeijer, Thin Solid Films 418 (2002) 89.
[20] L.P.H. Jeurgens, W.G. Sloof, F.D. Tichelaar, E.J. Mittemeijer, J. Appl. Phys. 92 (2002) 1649.
[21] G. Kresse, M. Schmid, E. Napetschnig, M. Shishkin, L. Kohler, P. Varga, Science 308 (2005) 1440.
[22] R.M. Jaeger, H. Kuhlenbeck, H.-J. Freund, Surf. Sci. 259 (1991) 235.
[23] J. Libuda, F. Winkelmann, M. Baumer, H.-J. Freund, T. Bertrams, H. Neddermeyer, K. Muller, Surf. Sci. 318 (1994) 61.
[24] M. Frank, K. Wolter, N. Magg, M. Heemeier, R. Kuhnemuth, M. Baumer, H.-J. Freund, Surf. Sci. 492 (2001) 270.
[25] M. Kulawik, N. Nilius, H.-P. Rust, H.-J. Freund, Phys. Rev. Lett. 91 (2003) 256101.
[26] X. Torrelles, F. Wendler, O. Bikondoa, H. Isern, W. Moritzb, G.R. Castro, Surf. Sci. 487 (2001) 97.
[27] A. Stierle, F. Renner, R. Streitel, H. Dosch, W. Drube, B.C. Cowie, Science 303 (2004) 1652.
[28] A. Stierle, V. Formoso, F. Comin, R. Franchy, Surf. Sci. 467 (2000) 85.
[29] R. Franchy, Surf. Sci. Rep. 38 (2000) 195.
[30] P. Gabmann, R. Franchy, H. Ibach, J. Electron. Spectrosc. Relat. Phenom. 64–65 (1993) 315.
[31] P. Gabmann, R. Franchy, H. Ibach, Surf. Sci. 319 (1994) 95.
[32] N. Cabrera, N.F. Mott, Rep. Prog. Phys. 12 (1949) 163.
[33] H. Graupner, L. Hammer, K. Heinz, D.M. Zehner, Surf. Sci. 380 (1997) 335.
[34] F.L. Battye, J.G. Jenkin, J. Liesegang, R.C.G. Leckey, Phys. Rev. B 9 (1974) 2887.
[35] Z.W. Lu, S.-H. Wei, A. Zunger, Acta Metall. Mater. 40 (1992) 2155.
[36] L.P.H. Jeurgens, W.G. Sloof, F.D. Tichelaar, E.J. Mittemeijer, Surf. Sci. 506 (2002) 313.
[37] A. Jimenez-Gonzalez, D. Schmelsser, Surf. Sci. 250 (1991) 59.
[38] CRC Press, Raton, FL, 1971/1972.
[39] P.C. Snijders, L.P.H. Jeurgens, W.G. Sloof, Surf. Sci. 496 (2002) 97.
[40] N. Cai, G.W. Zhou, K. Muller, D.E. Starr, Phys. Rev. Lett. 107 (2011) 035502.
[41] N. Cai, G.W. Zhou, K. Muller, D.E. Starr, Phys. Rev. B 84 (2011) 125445.
[42] N. Cai, G.W. Zhou, K. Muller, D.E. Starr, Appl. Phys. Lett. 101 (2012) 171605.